

# A $Z_4$ symmetric inverse seesaw model for neutrino masses and FIMP dark matter

Ziye Wang<sup>a,1</sup>, Yakefu Reyimuaji<sup>a,2</sup>, Nijiati Yalikun<sup>a,3</sup>

<sup>a</sup> *School of Physical Science and Technology, Xinjiang University, Urumqi 830017, China*

## Abstract

A theoretical framework based on a spontaneously broken  $Z_4$  symmetry is proposed to generate neutrino masses via the inverse seesaw mechanism and to facilitate dark matter production through a freeze-in scenario. The model introduces right-handed neutrinos  $N_i$ , additional fermions  $\chi_i$ , and a complex scalar  $S$ . The stability of the dark matter candidate is ensured by an unbroken  $Z_2$  subgroup, and its relic abundance is predominantly produced through decay and scattering processes involving the heavy singlet fermions. Phenomenological analyses show that this relatively minimal construction naturally aligns the neutrino oscillation parameters with the latest global oscillation data. Furthermore, the observed dark matter relic density is successfully accounted for within the overlapping parameter space relevant to neutrino properties.

---

<sup>1</sup>Email: zyewang@163.com

<sup>2</sup>Email: yreyi@hotmail.com

<sup>3</sup>Email: nijiaty@xju.edu.cn

# 1 Introduction

The quest to discovery of new physics beyond the Standard Model (SM) has led to profound inquiries into both the origin of neutrino masses and the nature of dark matter (DM). Neutrino oscillation experiments have conclusively demonstrated that neutrinos possess non-zero masses and mix among different flavors [1, 2]. Existence of the DM is validated indirectly through astronomical and cosmological observations [3–5], yet its particle nature remains elusive. These compelling challenges have motivated the exploration of various theoretical frameworks that can simultaneously address neutrino masses and DM.

Among the mechanisms proposed to generate neutrino masses, the seesaw mechanisms stand out due to their ability to naturally explain the smallness of neutrino masses by introducing heavy states of mass around  $10^{14}$  GeV. The inverse seesaw mechanism, in particular, offers a compelling alternative by introducing additional singlet fermions and allowing for several TeV-scale mediators, thereby making the scenario testable at current and future collider experiments [6–8]. This mechanism typically involves a richer fermion sector, which can also accommodate DM candidates under suitable symmetry protections [9–19].

DM production mechanisms are broadly categorized into two scenarios: freeze-out [20–26] and freeze-in [27–38]. While the freeze-out mechanism involves DM particles initially in thermal equilibrium with the SM plasma and subsequently decoupling as the universe expands, the freeze-in mechanism posits that DM particles were never in thermal equilibrium and their abundance was gradually accumulated through feeble interactions. The freeze-in scenario, often associated with Feebly Interacting Massive Particles (FIMPs), is particularly attractive as it does not require DM to have sizable couplings with the SM particles, thereby evading stringent experimental constraints.

Symmetries play a pivotal role in constructing models that can simultaneously address neutrino masses and DM. Discrete symmetries, such as  $Z_n$  groups, are instrumental in stabilizing DM candidates by forbidding their decay into SM particles [39–43]. In this work, we explore a model based on a spontaneously broken  $Z_4$  symmetry, which naturally leads to an unbroken  $Z_2$  subgroup responsible for DM stability. The  $Z_4$  symmetry ensures that while the SM fields are invariant, the new fermions transform non-trivially, thereby preventing undesirable interactions and stabilizing the lightest  $Z_2$ -odd particle.

Our primary objective is to elucidate how this minimal extension can simultaneously account for the observed neutrino masses via the inverse seesaw mechanism and generate the correct relic abundance of DM through the freeze-in process. The heavy singlet fermions  $N_i$  and  $\chi_i$  facilitate the inverse seesaw, with their interactions mediated by the scalar  $S$ . The freeze-in production of DM is predominantly governed by the decays and scatterings of these heavy states into the scalar and the DM candidate.

The structure of this paper is as follows: In section 2, we delineate the model framework, detailing the field content, symmetry assignments, and the resultant mass matrices. Section 3 is devoted to the phenomenological analysis, where we compute the neutrino mass spectrum and mixing parameters, and investigate the freeze-in production mechanisms for DM, including both decay and scattering processes. Numerical results are presented to demonstrate the viability of the model in aligning with current experimental observations. Finally, section 4 summarizes our findings and outlines potential avenues for future research. A supplemental details of a perturbative diagonalization of the heavy sector mass matrix are presented in the appendix A.

## 2 The model description

Here, we present a model that extends the SM by incorporating a  $Z_4$  symmetry. In this framework, all SM fields, except for the leptons, remain invariant under this symmetry. The model introduces new fields that are invariant under the SM symmetries, including right-handed neutrinos  $N_i$ , the right-handed fermions  $\chi_i$ , and a complex scalar field  $S$ . The scalar field  $S$  may acquire a nonzero vacuum expectation value (vev), consequently leading to the spontaneous breaking of the  $Z_4$  symmetry to its subgroup  $Z_2$ . The field content and the corresponding transformations under the electroweak gauge symmetries of the SM, the broken  $Z_4$  symmetry, as well as the unbroken  $Z_2$ , are summarized in table 1.

Fields	$L$	$e_R$	$N$	$\chi$	$S$	$H$
$SU_L$	2	1	1	1	1	2
$U(1)_Y$	$-\frac{1}{2}$	-1	0	0	0	$\frac{1}{2}$
$Z_4 \rightarrow Z_2$	$z \rightarrow -1$	$z \rightarrow -1$	$z \rightarrow -1$	$z^3 \rightarrow -1$	$z^2 \rightarrow 1$	$1 \rightarrow 1$

**Table 1:** Field content of the model and their transformations under the SM electroweak symmetry, the spontaneously broken  $Z_4$  symmetry, and the unbroken  $Z_2$  symmetry, where  $z$  denotes a quartic root of unity. All other SM fields remain singlets under these symmetries.

The interactions between fermions and scalars are encapsulated in the following Lagrangian,

$$\mathcal{L} = Y_E \bar{L} e_R H + Y_\nu \bar{L} N \tilde{H} + M \bar{N}^c \chi + \lambda S \bar{\chi}^c \chi + \lambda' S \bar{N}^c N + \text{h.c.} \quad (1)$$

where  $\tilde{H} = i\sigma_2 H^*$ . The first term corresponds to the charged lepton mass matrix, analogous to SM, with the mass given by  $m_E = Y_E \langle H \rangle$ . The Lagrangian presents several noteworthy features. The Majorana mass term for the right-handed neutrino is prohibited by the  $Z_4$  symmetry but is subsequently generated following spontaneous symmetry breaking, when the scalar field  $S$  acquires a vev  $\langle S \rangle$ . Similarly, the mass term for the singlet fermion  $\chi$  is also forbidden by the  $Z_4$  symmetry and emerges after symmetry breaking. The masses arising from the last two terms in eq. (1) are expected to be suppressed relative to the electroweak scale. In contrast, the  $Z_4$  symmetry permits the mass term  $M$ , which is anticipated to be several orders of magnitude larger than the electroweak scale. The small Majorana mass terms for  $N$  and  $\chi$  can originate in two distinct ways: either the couplings are intrinsically small while  $\langle S \rangle$  is sizable, or the couplings are of order unity with a correspondingly tiny vev. In this study, we consider the former scenario, which is natural from the perspective of symmetry enhancement in the limit where these couplings vanish. Specifically, when the couplings  $\lambda$  and  $\lambda'$  are set to zero, the symmetry of the model is enhanced to a  $U(1)$  symmetry. For example, in the absence of these couplings, the model exhibits a  $U(1)_L$  symmetry corresponding to lepton number conservation, with  $\chi$  assigned a lepton number of  $-1$  and all other leptons assigned a lepton number of  $+1$ .

According to 't Hooft's naturalness principle [44], the smallness of  $\lambda$  and  $\lambda'$  is technically natural, as their vanishing increases the symmetry of the theory. Furthermore, quantum corrections to these couplings are proportional to  $\lambda$  and  $\lambda'$  themselves, thereby preventing large radiative corrections. Consequently, these couplings remain small, stabilized by the enhanced symmetries when they are set to zero. The suppressed mass terms for the singlet fermion  $\chi$ , induced by these small couplings, are crucial for generating the small neutrino

masses via the inverse seesaw mechanism and are essential for  $\chi$  as a candidate for feebly interacting DM.

The inverse seesaw mechanism is illustrated in figure 1. By integrating out the heavy fermionic states  $N$  and  $\chi$  from the internal lines, this mechanism effectively induces a dimension-five operator of the form  $(LH)(LH)/\Lambda$ , commonly known as the Weinberg operator [45]. In this notation, the antisymmetric combination  $LH \equiv L_r \epsilon_{rs} H_s$  (with  $r, s = 1, 2$ ) denotes the contraction between the lepton and Higgs doublets. The resulting neutrino mass matrix obtained from the effective operator depicted in figure 1 reads:

$$m_\nu \simeq (\langle H \rangle^2 \langle S \rangle) Y_\nu (M^T)^{-1} \lambda M^{-1} Y_\nu^T, \quad (2)$$

where  $\langle H \rangle$  and  $\langle S \rangle$  denote the vevs of the Higgs and an additional scalar field, respectively. The smallness of  $m_\nu$  emerges from the second power suppression by the large mass scale  $M$  and the small Yukawa coupling  $\lambda$ , thereby naturally accommodating the observed neutrino masses within the inverse seesaw framework. At the core of the inverse seesaw mechanism

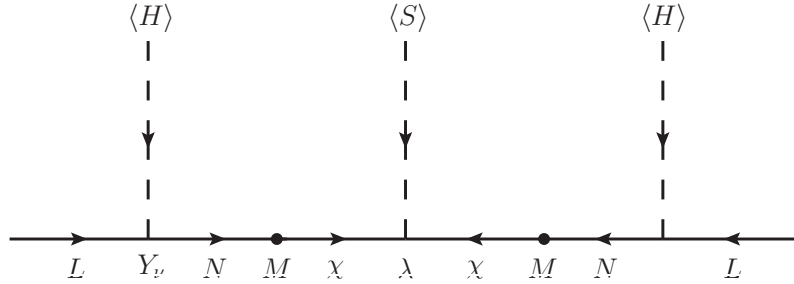


**Figure 1:** The Feynman diagram for the light neutrino mass generation via the inverse Seesaw mechanism

is the generation of light neutrino masses through a dual suppression structure. Specifically, the neutrino mass is simultaneously reduced by the large mass scale  $M$  and its dependence on the small mass term associated with the singlet fermion  $\chi$ . This structure ensures that the neutrino Dirac Yukawa couplings can remain of order unity, circumventing the need for it to be an exceedingly small parameter. Furthermore, unlike the conventional seesaw mechanism, which typically requires an extremely high mass scale, the inverse seesaw operates at comparatively lower energies. This not only preserves the naturalness of the Yukawa interactions but also renders the mechanism potentially testable in future experiments. In this manner, the inverse seesaw framework accommodates the observed smallness of neutrino masses while maintaining experimentally accessible scales and retaining viable parameter ranges for the underlying couplings.

The scalar potential, invariant under the considered symmetries, is given by

$$V(H, S) = -\mu_H^2 |H|^2 - \mu_S^2 |S|^2 + \frac{\lambda_H}{2} |H|^4 + \frac{\lambda_S}{2} |S|^4 + \lambda_{H,S} |H|^2 |S|^2, \quad (3)$$

where all coupling constants are real. For the potential to be bounded from below, the quartic couplings have to satisfy the conditions  $\lambda_H \geq 0$ ,  $\lambda_S \geq 0$  and  $\lambda_{H,S} \geq -2\sqrt{\lambda_H \lambda_S}$ . The scalar vevs break different symmetries at distinct energy scales. At higher energies, the singlet scalar acquires a vev  $\langle S \rangle$ , spontaneously breaking the  $Z_4$  symmetry down to its  $Z_2$  subgroup. Subsequently, at lower energies, the SM Higgs field obtains a  $\langle H \rangle$ , thereby breaking the

electroweak symmetry of the SM. To analyze the symmetry breaking, we expand the Higgs doublet and the singlet scalar around their respective vevs in the unitary gauge,

$$H = \frac{1}{\sqrt{2}} \begin{pmatrix} 0 \\ v + \phi_H \end{pmatrix}, \quad S = \frac{1}{\sqrt{2}}(u + \phi_S)e^{i\varphi}, \quad (4)$$

where the vevs  $\langle S \rangle = u/\sqrt{2}$  and  $\langle H \rangle = v/\sqrt{2}$  are assumed. The minimization conditions of the potential yield

$$\mu_H^2 = \frac{1}{2} (\lambda_H v^2 + \lambda_{H,S} u^2), \quad (5)$$

$$\mu_S^2 = \frac{1}{2} (\lambda_S u^2 + \lambda_{H,S} v^2). \quad (6)$$

The mass-squared matrix for the scalar fields is then

$$\mathcal{M}^2 = \begin{pmatrix} \lambda_H v^2 & \lambda_{H,S} v u \\ \lambda_{H,S} v u & \lambda_S u^2 \end{pmatrix}. \quad (7)$$

Diagonalizing this matrix results in two nonzero mass spectrum,

$$m_h^2 = \frac{1}{2} \left[ \lambda_H v^2 + \lambda_S u^2 - \sqrt{(\lambda_H v^2 - \lambda_S u^2)^2 + (2\lambda_{H,S} v u)^2} \right], \quad (8)$$

$$m_\phi^2 = \frac{1}{2} \left[ \lambda_H v^2 + \lambda_S u^2 + \sqrt{(\lambda_H v^2 - \lambda_S u^2)^2 + (2\lambda_{H,S} v u)^2} \right], \quad (9)$$

corresponding to the mass eigenstates  $h$  and  $\phi$ , respectively. Here,  $h$  is identified as the SM-like Higgs boson, and  $\phi$  as a heavier scalar. Given that  $u \gg v$ , the masses can be approximated as

$$m_h^2 \approx \left( \lambda_H - \frac{\lambda_{H,S}^2}{\lambda_S} \right) v^2, \quad m_\phi^2 \approx \lambda_S u^2 + \frac{\lambda_{H,S}^2}{\lambda_S} v^2. \quad (10)$$

From these expressions, it is evident that the SM Higgs mass and the singlet scalar mass are restored when the scalar mixing coupling  $\lambda_{H,S}$  is set to zero. The linear transformations between the original scalar fields and the mass eigenstates are given by

$$h = \phi_H \cos \theta - \phi_S \sin \theta, \quad (11)$$

$$\phi = \phi_S \cos \theta + \phi_H \sin \theta, \quad (12)$$

where the orthogonal rotation angle  $\theta$  satisfies

$$\tan \theta = \frac{\lambda_S u^2 - \lambda_H v^2}{2\lambda_{H,S} v u} \left[ \sqrt{1 + \frac{(2\lambda_{H,S} v u)^2}{(\lambda_S u^2 - \lambda_H v^2)^2}} - 1 \right]. \quad (13)$$

Considering the hierarchy  $u \gg v$ , this expression can be approximated as

$$\tan \theta \approx \frac{v\lambda_{H,S}}{u\lambda_S} \left[ 1 + \frac{v^2}{\lambda_S u^2} \left( \lambda_H - \frac{\lambda_{H,S}^2}{\lambda_S} \right) \right]. \quad (14)$$

It is clear that the mixing angle  $\theta$  vanishes when the coupling  $\lambda_{H,S}$  is set to zero. In this limit, the SM Higgs mass reverts to its standard form, and the scalar sector consists solely of an additional self-interacting singlet scalar that does not interact with the Higgs boson. Under these conditions, an upper bound for the mixing angle can be established,  $\sin \theta < 0.1$  [46–49]. Such a small mixing is insufficient to produce observable effects in collider experiments, including Higgs factories.

### 3 The phenomenological aspects

#### 3.1 Neutrino mass and mixing from the inverse seesaw mechanism

The Yukawa interactions in eq. (1) generate fermion masses upon the scalars get vevs. The mass matrix derived from the relevant part of the Lagrangian is given by

$$\mathcal{L}_m = (\bar{L} \quad \bar{N}^c \quad \bar{\chi}^c) \begin{pmatrix} 0 & m_D & 0 \\ m_D^T & \mu' & M \\ 0 & M^T & \mu \end{pmatrix} \begin{pmatrix} L \\ N \\ \chi \end{pmatrix}, \quad (15)$$

where each entry is  $3 \times 3$  matrices, with  $m_D = \frac{v}{\sqrt{2}}Y_\nu$ ,  $\mu = \frac{\lambda}{\sqrt{2}}u$ , and  $\mu' = \frac{\lambda'}{\sqrt{2}}u$ . The  $Z_4$  symmetry prohibits the Majorana mass terms  $\mu$  and  $\mu'$  for the right-handed singlet fermions, ensuring that these masses are naturally smaller than the electroweak scale mass term  $m_D$ . Furthermore,  $m_D$  itself is much smaller than the symmetry-allowed mass term  $M$ . This hierarchical structure,  $\mu, \mu' \ll m_D \ll M$ , satisfies the conditions necessary for the inverse seesaw mechanism.

The full mass matrix can be decomposed into four blocks

$$\mathcal{M} = \begin{pmatrix} 0 & m_D & 0 \\ m_D^T & \mu' & M \\ 0 & M^T & \mu \end{pmatrix} = \begin{pmatrix} 0 & \mathcal{M}_D \\ \mathcal{M}_D^T & \mathcal{M}_N \end{pmatrix}, \quad (16)$$

where  $\mathcal{M}_D = (m_D \quad 0)$ , and

$$\mathcal{M}_N = \begin{pmatrix} \mu' & M \\ M^T & \mu \end{pmatrix}. \quad (17)$$

To determine the light neutrino mass matrix within the seesaw framework, it is necessary to compute the inverse of the  $\mathcal{M}_N$  block. Assuming that  $M$  is non-singular, its inverse is

$$\mathcal{M}_N^{-1} = \begin{pmatrix} -(M^T - \mu M^{-1}\mu')^{-1} \mu M^{-1} & (M^T - \mu M^{-1}\mu')^{-1} \\ (M - \mu'(M^T)^{-1}\mu)^{-1} & -M^{-1}\mu'(M^T - \mu M^{-1}\mu')^{-1} \end{pmatrix}. \quad (18)$$

Applying the block diagonalization procedure, the light neutrino mass matrix is obtained as

$$m_\nu = -\mathcal{M}_D \mathcal{M}_N^{-1} \mathcal{M}_D^T = m_D (M^T - \mu M^{-1}\mu')^{-1} \mu M^{-1} m_D^T \quad (19)$$

Given the hierarchy  $\mu, \mu' \ll M$ , we retain only the leading order terms in  $\mu$  and  $\mu'$ , neglecting the second term within the parentheses. This simplification yields

$$m_\nu = m_D (M^T)^{-1} \mu M^{-1} m_D^T, \quad (20)$$

which is consistent with the result obtained from the effective field theory approach in eq. (2). The neutrino mass matrix  $m_\nu$  is proportional to the small mass parameter  $\mu$  and is doubly suppressed by the mass scale  $M$ , characteristic of the inverse seesaw mechanism. It should be emphasized that this result extends to scenarios involving more than three generations. Conversely, they are equally applicable to cases with only one or two generations. For the single-generation case, the mass matrix simplifies to

$$m_\nu = \frac{y_\nu^2}{2M^2} v^2 \mu, \quad (21)$$

indicating that a Majorana mass term  $\mu \sim \mathcal{O}(10)$  eV is required for  $M \sim \mathcal{O}(10)$  TeV, assuming natural values for the neutrino Yukawa coupling.

The block diagonalization of the mass matrix  $\mathcal{M}$  in eq. (16) is performed using the rotation matrix

$$\mathcal{U} = \begin{pmatrix} \mathbf{I}_3 - \frac{1}{2}\epsilon\epsilon^T & \epsilon \\ -\epsilon^T & \mathbf{I}_3 - \frac{1}{2}\epsilon^T\epsilon \end{pmatrix}, \quad (22)$$

where  $\epsilon = \mathcal{M}_D \mathcal{M}_N^{-1} = (-m_\nu(m_D^T)^{-1}, m_D(M^T)^{-1})$ . Applying this rotation, the mass matrix is block diagonalized as

$$\mathcal{U}^T \mathcal{M} \mathcal{U} = \begin{pmatrix} -\mathcal{M}_D \mathcal{M}_N^{-1} \mathcal{M}_D^T & \\ & \mathcal{M}_N + \frac{1}{2} \left[ \mathcal{M}_D^T (\mathcal{M}_D \mathcal{M}_N^{-1}) + (\mathcal{M}_D \mathcal{M}_N^{-1})^T \mathcal{M}_D \right] \end{pmatrix}, \quad (23)$$

to leading order in  $\mathcal{M}_D \mathcal{M}_N^{-1}$ . The mixing between the light and heavy sectors is characterized by the small parameter  $\epsilon$ , and each diagonal block in eq. (23) isolates the light and heavy mass spectra. The small corrections to  $\mathcal{M}_N$  can be safely neglected in subsequent analyses.

To fully diagonalize the mass matrix, further unitary transformations are performed on each block. Specifically, two additional unitary matrices  $V_\nu$  and  $V_N$  are introduced such that

$$\begin{aligned} V_\nu^T m_\nu V_\nu &= \text{diag}(m_1, m_2, m_3), \\ V_N^T \mathcal{M}_N V_N &= \text{diag}(M_1, \dots, M_6), \end{aligned} \quad (24)$$

where  $(m_1, m_2, m_3)$  are the masses of the light neutrinos and  $(M_1, \dots, M_6)$  are the masses of the heavy singlet states.

The Pontecorvo-Maki-Nakagawa-Sakata (PMNS) mixing matrix  $U_{\text{PMNS}}$  is then given by

$$U_{\text{PMNS}} = U_l^\dagger (\mathbf{I}_3 - \frac{1}{2}\epsilon\epsilon^T) V_\nu, \quad (25)$$

where  $U_l$  diagonalizes the Hermitian combination of the charged lepton mass matrix, satisfying  $U_l^\dagger m_E m_E^\dagger U_l = \text{diag}(m_e^2, m_\mu^2, m_\tau^2)$ . The term  $\frac{1}{2}\epsilon\epsilon^T$  quantifies the deviation from unitarity in the PMNS matrix. However, since this deviation is quadratic in  $\epsilon$ , its contribution is negligible and can be ignored in the following discussions.

The masses of the heavy singlet fermions are determined through the diagonalization of the mass matrix, expressed as  $Q^T \mathcal{M}_N Q = D$ , where  $Q$  is a unitary matrix and  $D$  is a diagonal matrix with non-negative entries. Given the hierarchical structure  $\mu, \mu' \ll M$ , a perturbative diagonalization method is employed. A comprehensive calculation is provided in the appendix A, where, for simplicity, the off-diagonal block matrix  $M$  is assumed to be real. Following diagonalization, significant mixing between the singlets  $N$  and  $S$  is observed, resulting in three pairs of degenerate masses. This degeneracy persists even when first-order perturbations  $\mu M^{-1}$  and  $\mu' M^{-1}$  are included. However, the degeneracy is lifted when second-order perturbations are considered, implying that the three pairs of singlet fermions possess closely spaced masses.

Concerning the neutrino masses, the mass matrix in eq. (20) must be diagonalized. To determine the leptonic mixing, the rotation matrices  $U_l$  and  $V_\nu$  are calculated from the diagonalization of the charged lepton and neutrino mass matrices, respectively. To facilitate this process, we construct a flavor symmetry model based on the simplest non-Abelian group,

$S_3$ , defined by two generators  $\{S, T | S^2 = T^2 = (ST)^3 = e\}$ . This group comprises two one-dimensional and one two-dimensional irreducible representations, with the following multiplication rules:

$$\begin{aligned} 1 \times r &= r, \quad r \in \{1, 1', 2\}, \\ 1' \times 1' &= 1, \quad 1' \times 2 = 2, \\ 2 \times 2 &= 1 + 1' + 2. \end{aligned} \quad (26)$$

In the  $\rho(T)$ -diagonal basis of the group representation, the Clebsch-Gordan decompositions for the product of two doublets  $(x_1, y_1)$  and  $(x_2, y_2)$  are given by [50, 51]:

$$1 \sim x_1 y_1 + x_2 y_2, \quad 1' \sim x_1 y_2 - x_2 y_1, \quad 2 \sim \begin{pmatrix} x_1 y_2 + x_2 y_1 \\ x_1 y_1 - x_2 y_2 \end{pmatrix}. \quad (27)$$

To further constrain the mass matrices, an additional  $Z_2$  symmetry is imposed under which  $L_1$ ,  $e_{1,R}$  and  $N_3$  are odd, while all other fields are even. Under  $S_3$ , the field assignments are as follows:  $L_1 \sim 1'$ ,  $L_D \equiv (L_2, L_3) \sim 2$ ,  $e_{1,R} \sim 1'$ ,  $\ell_R \equiv (e_{2,R}, e_{3,R}) \sim 2$ , and a flavon  $\varphi = (\varphi_1, \varphi_2) \sim 2$ . These assignments restrict the charged lepton Yukawa Lagrangian to

$$\mathcal{L}_E = Y_{E11}(\bar{L}_1 H) e_{1,R} + Y_{E22} [(\bar{L}_D H) \ell_R]_1 + \frac{Y_{E23}}{\Lambda} [(\bar{L}_D H) \ell_R \varphi]_1 + \text{h.c.}, \quad (28)$$

where  $\Lambda$  is the cutoff scale of the flavor model, and the subscript 1 of the square bracket denotes the singlet combination. With the vev alignment  $\langle \varphi \rangle = v_\varphi (1, 0)^T$ , the charged lepton mass matrix is given by

$$m_E = \begin{pmatrix} a_1 & 0 & 0 \\ 0 & a_2 & -a_3 \\ 0 & -a_3 & a_2 \end{pmatrix}, \quad (29)$$

where  $a_1 = Y_{E11} \langle H \rangle$ ,  $a_2 = Y_{E22} \langle H \rangle$  and  $a_3 = -Y_{E23} \langle H \rangle v_\varphi / \Lambda$ .

Considering the representations  $N_D \equiv (N_1, N_2) \sim 2$ ,  $N_3, \chi_1 \sim 1'$ ,  $\chi_D \equiv (\chi_2, \chi_3) \sim 2$ , the Yukawa Lagrangian responsible for neutrino masses is constructed as

$$\begin{aligned} \mathcal{L}_\nu &= Y_{\nu 13} \bar{L}_1 N_3 \tilde{H} + Y_{\nu 21} \bar{L}_D N_D \tilde{H} + \frac{Y_{\nu 22}}{\Lambda} [\bar{L}_D N_D \tilde{H} \varphi]_1 + \lambda_{11} S \bar{\chi}_1^c \chi_1 + \lambda_{22} S \bar{\chi}_D^c \chi_D \\ &+ \frac{\lambda_{13}}{\Lambda} S \bar{\chi}_1^c [\chi_D \varphi]_{1'} + \frac{\lambda_{13}}{\Lambda} S [\bar{\chi}_D^c \varphi]_{1'} \chi_1 + \frac{\lambda_{23}}{\Lambda} S [\bar{\chi}_D^c \chi_D \varphi]_1 \\ &+ M_{31} \bar{N}_3^c \chi_1 + M_{12} \bar{N}_D^c \chi_D + \text{h.c.} \end{aligned} \quad (30)$$

The subscript indices on the terms involving  $\varphi$  indicate the specific  $S_3$  singlet combinations. The flavor symmetry imposes the following structures on the mass matrices:

$$\begin{aligned} m_D &= \frac{v}{\sqrt{2}} \begin{pmatrix} 0 & 0 & Y_{\nu 13} \\ Y_{\nu 21} & Y_{\nu 22} \frac{v_\varphi}{\Lambda} & 0 \\ Y_{\nu 22} \frac{v_\varphi}{\Lambda} & Y_{\nu 21} & 0 \end{pmatrix}, \quad M = \begin{pmatrix} 0 & M_{12} & 0 \\ 0 & 0 & M_{12} \\ M_{31} & 0 & 0 \end{pmatrix}, \\ \mu &= \frac{u}{\sqrt{2}} \begin{pmatrix} \lambda_{11} & 0 & -\lambda_{13} \frac{v_\varphi}{\Lambda} \\ 0 & \lambda_{22} & \lambda_{23} \frac{v_\varphi}{\Lambda} \\ -\lambda_{13} \frac{v_\varphi}{\Lambda} & \lambda_{23} \frac{v_\varphi}{\Lambda} & \lambda_{22} \end{pmatrix}. \end{aligned} \quad (31)$$



In this expressions, we neglect the flavon-induced corrections to the mass matrix  $M$  due to the large magnitude of its entries corresponding to the heavy masses. Consequently, the light neutrino mass matrix is given by

$$m_\nu = \frac{uv^2}{2\sqrt{2}} \begin{pmatrix} \frac{Y_{\nu 13}^2 \lambda_{11}}{M_{31}^2} & -\frac{Y_{\nu 13} Y_{\nu 22} \lambda_{13}}{M_{12} M_{31}} r^2 & -\frac{Y_{\nu 13} Y_{\nu 21} \lambda_{13}}{M_{12} M_{31}} r \\ -\frac{Y_{\nu 13} Y_{\nu 22} \lambda_{13}}{M_{12} M_{31}} r^2 & \frac{Y_{\nu 21}^2 \lambda_{22} + (Y_{\nu 22}^2 \lambda_{22} + 2Y_{\nu 21} Y_{\nu 22} \lambda_{23}) r^2}{M_{12}^2} & \frac{2Y_{\nu 21} Y_{\nu 22} \lambda_{22} + Y_{\nu 21}^2 \lambda_{23} + r^2 Y_{\nu 22}^2 \lambda_{23}}{M_{12}^2} r \\ -\frac{Y_{\nu 13} Y_{\nu 21} \lambda_{13}}{M_{12} M_{31}} r & \frac{2Y_{\nu 21} Y_{\nu 22} \lambda_{22} + Y_{\nu 21}^2 \lambda_{23} + r^2 Y_{\nu 22}^2 \lambda_{23}}{M_{12}^2} r & \frac{Y_{\nu 21}^2 \lambda_{22} + (Y_{\nu 22}^2 \lambda_{22} + Y_{\nu 21} Y_{\nu 22} \lambda_{23}) r^2}{M_{12}^2} \end{pmatrix}, \quad (32)$$

where  $r = \frac{v_\varphi}{\Lambda}$ . Given the complexity of this mass matrix structure, extracting physical quantities in a generic form is challenging. Therefore, for illustrative purposes, we adopt a highly constrained form characterized by three parameters:

$$\tilde{m}_\nu = \begin{pmatrix} 12\mu_2 + \frac{1}{4}(\mu_1 + \mu_2)e^{2i\alpha} & \mu_1 & -\sqrt{3}[\mu_2 - (\mu_1 + \mu_2)e^{2i\alpha}]e^{-i\alpha} \\ \mu_1 & \frac{7}{4}(\frac{2}{3}\mu_1 + 7\mu_2) & -\frac{\mu_1}{4\sqrt{3}}e^{-i\alpha} \\ -\sqrt{3}[\mu_2 - (\mu_1 + \mu_2)e^{2i\alpha}]e^{-i\alpha} & -\frac{\mu_1}{4\sqrt{3}}e^{-i\alpha} & 12(\mu_1 + \mu_2) + \frac{1}{4}\mu_2 e^{-2i\alpha} \end{pmatrix}, \quad (33)$$

where  $\mu_1$  and  $\mu_2$  are real parameters with mass dimension one, and  $\alpha$  is a dimensionless parameter. To determine the neutrino masses, we first diagonalize the charged lepton mass matrix in eq (29),  $U_l^\dagger m_E U_r = \text{diag}(m_e, m_\mu, m_\tau)$ , which is achieved by

$$U_l = \begin{pmatrix} 1 & 0 & 0 \\ 0 & \frac{1}{\sqrt{2}} & -\frac{1}{\sqrt{2}} \\ 0 & \frac{1}{\sqrt{2}} & \frac{1}{\sqrt{2}} \end{pmatrix}, \quad U_r = U_l P, \quad (34)$$

$$m_e = |a_1|, \quad m_\mu = |a_2 - a_3|, \quad m_\tau = |a_2 + a_3|,$$

where  $P = \text{diag}(\text{sign}(a_1), \text{sign}(a_2 - a_3), \text{sign}(a_2 + a_3))$ . On the other hand, the neutrino mass matrix is diagonalized as  $V_\nu^T \tilde{m}_\nu V_\nu = \text{diag}(m_1, m_2, m_3)$ , where

$$V_\nu = \begin{pmatrix} \frac{6}{7} & \frac{2\sqrt{3}}{7} & \frac{1}{7}e^{-i\alpha} \\ -\frac{1}{2} & \frac{\sqrt{3}}{2} & 0 \\ -\frac{\sqrt{3}}{14}e^{i\alpha} & -\frac{1}{14}e^{i\alpha} & \frac{4\sqrt{3}}{7} \end{pmatrix}, \quad (35)$$

$$m_1 = \frac{7}{4} \left( 7\mu_2 - \frac{1}{3}\mu_1 \right), \quad m_2 = \frac{7}{4} (7\mu_2 + \mu_1), \quad m_3 = \frac{7^2}{4} (\mu_1 + \mu_2).$$

As demonstrated, the neutrino masses and mixing parameters are functions of the three real parameters  $\mu_{1,2}$  and  $\alpha$ . The deviation from unitarity, quantified by  $\epsilon e^T = \frac{1}{m_D^2} m_\nu m_\nu^T + \frac{1}{M^2} m_D m_D^T \sim \mathcal{O}(10^{-4})$ , is sufficiently small and can thus be neglected when computing the mixing matrix. Consequently, the leptonic mixing matrix, as defined in eq (25), is approximately given by

$$U_{\text{PMNS}} \approx \begin{pmatrix} \frac{6}{7} & \frac{2\sqrt{3}}{7} & \frac{1}{7}e^{-i\alpha} \\ -\frac{7+\sqrt{3}e^{i\alpha}}{14\sqrt{2}} & \frac{7\sqrt{3}-e^{i\alpha}}{14\sqrt{2}} & \frac{2\sqrt{6}}{7} \\ \frac{7-\sqrt{3}e^{i\alpha}}{14\sqrt{2}} & -\frac{7\sqrt{3}+e^{i\alpha}}{14\sqrt{2}} & \frac{2\sqrt{6}}{7} \end{pmatrix}. \quad (36)$$

The magnitudes of the elements of this mixing matrix are

$$|U_{\text{PMNS}}| = \begin{pmatrix} \frac{6}{7} & \frac{2\sqrt{3}}{7} & \frac{1}{7} \\ \frac{1}{14}\sqrt{26+7\sqrt{3}\cos\alpha} & \frac{1}{14}\sqrt{74-7\sqrt{3}\cos\alpha} & \frac{2\sqrt{6}}{7} \\ \frac{1}{14}\sqrt{26-7\sqrt{3}\cos\alpha} & \frac{1}{14}\sqrt{74+7\sqrt{3}\cos\alpha} & \frac{2\sqrt{6}}{7} \end{pmatrix}, \quad (37)$$

which aligns well with current neutrino oscillation data. For comparison, the ranges of each element obtained from our theoretical analysis and the current  $3\sigma$  global fit results [52, 53] are presented below:

$$\begin{aligned} |U_{\text{PMNS}}|_{\text{th}} &= \begin{pmatrix} 0.857 & 0.495 & 0.143 \\ 0.266 \rightarrow 0.441 & 0.562 \rightarrow 0.663 & 0.699 \\ 0.266 \rightarrow 0.441 & 0.562 \rightarrow 0.663 & 0.699 \end{pmatrix}, \\ |U_{\text{PMNS}}|_{\text{ex}} &= \begin{pmatrix} 0.801 \rightarrow 0.842 & 0.519 \rightarrow 0.580 & 0.142 \rightarrow 0.155 \\ 0.252 \rightarrow 0.501 & 0.496 \rightarrow 0.680 & 0.652 \rightarrow 0.756 \\ 0.276 \rightarrow 0.518 & 0.485 \rightarrow 0.673 & 0.637 \rightarrow 0.743 \end{pmatrix}. \end{aligned} \quad (38)$$

Comparing the structure of the mixing matrix in eq. (36) with its standard parameterization [54], we identify the three mixing angles and the Dirac CP-violating phase as

$$\sin\theta_{12} = \frac{1}{2}, \quad \sin\theta_{23} = \frac{\sqrt{2}}{2}, \quad \sin\theta_{13} = \frac{1}{7}, \quad \delta_{\text{CP}} = \alpha, \quad (39)$$

which correspond to  $\theta_{12} = 30^\circ$ ,  $\theta_{23} = 45^\circ$  and  $\theta_{13} = 8.2^\circ$ . The CP-violating phase  $\delta_{\text{CP}}$  remains unconstrained in this simple example. Although this simplified structure of the neutrino mass matrix captures the main features of the mixing angles, it does not fully conform to the experimental data. To achieve precise agreement with the observed oscillation parameters, one may need to refine the structure of the neutrino mass matrix by introducing small modifications.

### 3.2 Freeze-in dark matter

Regarding the additional singlet fermions  $N$  and  $\chi$ , the symmetries of the model forbid any interactions with other particles, except for the mixing of  $N$  with the left-handed neutrinos. These electrically neutral fermions undergo sign inversion under the unbroken  $Z_2$  symmetry. As  $Z_2$ -odd fermions, the lightest singlet is stable and thus constitutes a relic particle. Notably, the mixing between the heavy singlets and the SM neutrino is characterized by a small parameter  $\epsilon$ , which is expected to be negligible. Consequently, it is unlikely that these singlet fermions achieve thermal equilibrium with the SM plasma in the early universe, followed by a freeze-out as the temperature drops below their masses. Instead, the decoupled species either decay or annihilate into the lightest singlet, thereby gradually contributing to the DM abundance through the freeze-in mechanism and eventually attaining the observed relic density. This behavior is a fundamental feature of the freeze-in production mechanism for DM [27, 30, 55].

In our framework, the decoupled heavy singlets decay into lighter states and may annihilate when the temperature is sufficiently high. Due to their large masses and feeble interaction strengths, the lightest singlet fermion, denoted as  $\chi$ , serves as a candidate for DM in the form FIMP. Consistent with the freeze-in scenario, we assume that the heavy singlets  $N$

and  $\chi$  never attain thermal equilibrium with the SM thermal bath and that  $\chi$  possesses a negligible initial abundance. Subsequently, through decay and annihilation processes, the DM abundance of  $\chi$  increases and ultimately satisfies the observational constraints. In the following sections, we provide a detailed analysis of the production mechanisms of the FIMP  $\chi$  and compute its relic density.

### 3.2.1 Dark matter production through right-handed neutrino decay

One of the primary mechanisms for generating the DM candidate  $\chi$  involves the decay of heavy neutrinos  $N_i$  in association with the scalar particles  $h, \phi$ , specifically through the processes  $N_i \rightarrow \chi h$  and  $N_i \rightarrow \chi \phi$ . The corresponding Feynman diagrams for these decay channels are illustrated in figure 2. These decay processes can provide a non-negligible contribution to the

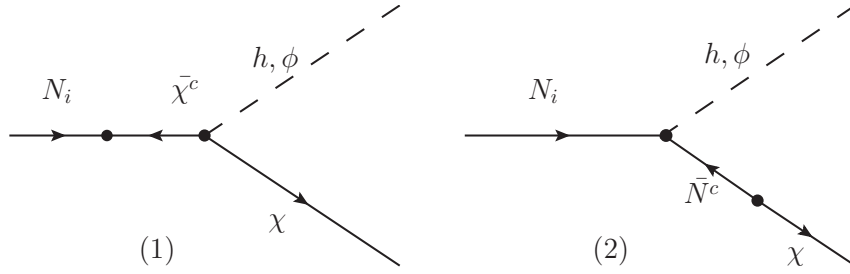


**Figure 2:** Production of DM via the decay of right-handed neutrinos  $N_i$ .

DM abundance due to the Yukawa coupling between  $\chi$  and the heavy singlets  $N$ , as well as the significant mixing between  $N$  and  $\chi$ . The yield of DM produced through this process is given by [27, 56]

$$Y_\chi \simeq 0.656 \frac{M_{\text{Pl}} (\Gamma_{N_i \rightarrow h\chi} + \Gamma_{N_i \rightarrow \phi\chi})}{g_{*S} \sqrt{g_*} M_{N_i}^2}, \quad (40)$$

where  $g_*$  and  $g_{*S}$  denote the effective numbers of relativistic degrees of freedom for energy density and entropy density, respectively, in the thermal bath when the temperature is approximately equal to the mass of the decaying particle  $M_{N_i}$ .  $M_{\text{Pl}}$  represents the Planck mass, and  $\Gamma_{N_i \rightarrow h\chi}$  and  $\Gamma_{N_i \rightarrow \phi\chi}$  are the decay widths of  $N_i$  into  $\chi h$  and  $\chi \phi$ , respectively. The decay widths can be calculated using the relevant Feynman rules, and their sum is expressed as

$$\Gamma_{N_i \rightarrow h\chi} + \Gamma_{N_i \rightarrow \phi\chi} = \frac{(m_N^4 - m_\chi^4)}{2^8 \pi m_N^3} [\lambda^2 + \lambda'^2 + \lambda\lambda'(1 + \sin 2\theta)], \quad (41)$$

where  $m_N$  and  $m_\chi$  are the masses of the heavy neutrino  $N$  and the DM candidate  $\chi$ , respectively. The parameters  $\lambda$  and  $\lambda'$  denote the Yukawa couplings, and  $\theta$  represents the scalar mixing angle. In this analysis, maximal mixing between the two singlets is assumed. This expression implies that the decay channels become kinematically forbidden when  $m_N = m_\chi$ , as the phase space for the decay vanishes. This outcome is consistent with kinematic expectations, where equal masses prevent the decay from occurring. Additionally, the contribution from the scalar mixing angle  $\theta$  is minimal due to its small magnitude.

In our analysis, we find that the decay of heavy neutrinos  $N_i$  into the DM candidate  $\chi$  and scalar particles  $h$  or  $\phi$  constitutes a significant production mechanism within this framework. The detailed computation of the DM yield  $Y_\chi$  accounts for the relevant decay widths and the thermal history of the early universe, adhering to the freeze-in production paradigm [27, 30, 55].

### 3.2.2 Dark matter production by scattering

Another process contributing to the production of the FIMP DM candidate  $\chi$  involves  $2 \rightarrow 2$  scattering processes. Specifically, these processes include  $\bar{\nu}h$  (or  $\phi$ )  $\rightarrow \chi h$  (or  $\phi$ ),  $\bar{\nu}N \rightarrow \chi\bar{\chi}^c$  and  $\bar{N}^c N \rightarrow \chi\bar{\chi}^c$ , as illustrated in figure 3.

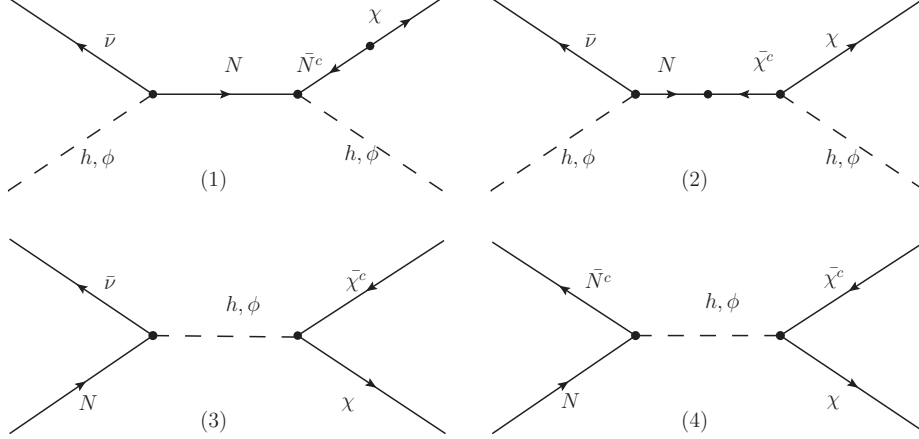


**Figure 3:** Production of DM via scattering processes.

The time evolution of the DM number density  $n_\chi$  is governed by the Boltzmann equation,

$$\frac{dn_\chi}{dt} + 3Hn_\chi = \int \frac{d^3p_a}{(2\pi)^3 2E_a} \frac{d^3p_b}{(2\pi)^3 2E_b} \frac{d^3p_\chi}{(2\pi)^3 2E_\chi} \frac{d^3p_c}{(2\pi)^3 2E_c} (2\pi)^4 \delta^4(p_a + p_b - p_\chi - p_d) |\mathcal{M}|^2 f_a f_b \quad (42)$$

where  $p_i$  and  $E_i$  denote the momenta and energies of the particles involved in the scattering process  $a + b \rightarrow \chi + c$ , and  $f_a$  and  $f_b$  are the distribution functions of the initial particles  $a$  and  $b$ . The right-hand side represents the collision term, which quantifies the rate at which DM particles are produced in the early universe through scattering processes, assuming that the initial DM abundance is negligible. The collision term can be expressed in terms of the number densities of the initial states and the thermally averaged cross section,

$$C = \int \frac{d^3p_a}{(2\pi)^3} \frac{d^3p_b}{(2\pi)^3} f_a f_b \sigma v_{\text{rel}} \simeq n_a n_b \langle \sigma v \rangle. \quad (43)$$

In figure 3, the first two diagrams involve the production of a single DM particle in the final state, whereas the last two diagrams correspond to the production of a DM particle pair. Given the substantial mass of the DM candidate, single DM production is feasible only when the initial state energy exceeds the DM mass. In contrast, pair production requires the initial energy to surpass twice the DM mass. When analyzing the contributions of these processes, it is reasonable to neglect the contributions from scalars and light neutrino masses. This simplification not only renders the computations more tractable but also provides an effective approximation. The subsequent analysis treats these processes separately.

The scattering cross sections for processes (1) and (2) in figure 3, mediated by a heavy singlet, are computed, and their sum is

$$\sigma(1+2) = \frac{(\lambda + \lambda')^2}{2^{11}\pi} |Y_\nu|^2 \frac{\cos^2(2\theta) m_N^2}{(s - m_N^2)^2}, \quad (44)$$

where  $s$  is the squared center-of-mass energy, and  $\theta$  is the scalar mixing angle. The thermally averaged cross section is given by

$$\langle\sigma v\rangle(1+2) = \frac{(\lambda + \lambda')^2 |Y_\nu|^2 \cos^2(2\theta) m_N^2}{2^{16} \pi T^5} \int_{m_\chi^2}^{\infty} \frac{s^{3/2}}{(s - m_N^2)^2} K_1\left(\frac{\sqrt{s}}{T}\right) ds. \quad (45)$$

where  $K_1$  is the modified Bessel function of the second kind of order one. Consequently, the collision term is expressed as

$$C(1+2) = \frac{3\zeta(3)^2 T}{2^{17} \pi^5} (\lambda + \lambda')^2 |Y_\nu|^2 \cos^2(2\theta) m_N^2 \int_{m_\chi^2}^{\infty} \frac{s^{3/2}}{(s - m_N^2)^2} K_1\left(\frac{\sqrt{s}}{T}\right) ds. \quad (46)$$

To solve the Boltzmann equation, we introduce the DM yield  $Y_\chi = \frac{n_\chi}{S}$ , a ratio of the number density to the entropy density  $S$ , as usually adopted in the literature. The Boltzmann equation then becomes

$$Y_\chi(1+2) = \int_0^\infty \frac{C(1+2)}{S H T} dT, \quad (47)$$

where the entropy density  $S$  and the Hubble parameter  $H$  during the radiation-dominated era are given by

$$\begin{aligned} S &= \frac{2\pi^2}{45} g_{*s} T^3, \\ H &= \frac{1.66 \sqrt{g_*} T^2}{M_{\text{Pl}}}. \end{aligned} \quad (48)$$

Substituting these expressions into eq. (47), the DM yield produced by processes (1) and (2) is

$$Y_\chi(1+2) = \frac{135\zeta(3)^2 (\lambda + \lambda')^2 |Y_\nu|^2 \cos^2(2\theta) m_N^2 M_{\text{Pl}}}{1.66 \times 2^{18} \pi^7 g_{*s} \sqrt{g_*}} \int_0^\infty \int_{m_\chi^2}^\infty \frac{s^{3/2}}{T^5 (s - m_N^2)^2} K_1\left(\frac{\sqrt{s}}{T}\right) ds dT. \quad (49)$$

For process (3), the scattering cross section is given by

$$\sigma(3) = \frac{\lambda^2 |Y_\nu|^2}{2^{13} \pi} \sin^2(2\theta) \sqrt{1 - \frac{4m_\chi^2}{s}} \left( \frac{1}{s - m_\phi^2} - \frac{1}{s - m_h^2} \right)^2 (s - 2m_\chi^2). \quad (50)$$

In this model, a mass hierarchy is assumed,  $m_N, m_\chi, m_\phi \gg m_h \gg m_\nu$ . The thermally averaged scattering cross section is derived by considering scenarios where a non-relativistic heavy right-handed neutrino  $N$  and a relativistic neutrino  $\bar{\nu}$  are involved in the initial state. Utilizing the assumed mass hierarchy, an approximate expression for the thermally averaged cross section is obtained as

$$\langle\sigma v\rangle(3) = \frac{15\lambda^2 |Y_\nu|^2 \sin^2(2\theta) m_\phi^4 (m_N^2 - 2m_\chi^2)}{2^{16} \sqrt{2\pi} m_N m_\phi^4 (m_N^2 - m_\phi^2)^2} T^{1/2}. \quad (51)$$

The corresponding collision term is thus

$$C(3) = \frac{45\zeta(3)\lambda^2 |Y_\nu|^2 \sin^2(2\theta) m_\phi^4 (m_N^2 - 2m_\chi^2)}{2^{18} \pi^4 m_N^3 (m_N^2 - m_\phi^2)^2} T^5 e^{-m_N/T}. \quad (52)$$

Substituting this expression into the Boltzmann equation and performing the temperature integration provides the DM yield

$$Y_\chi(3) = \frac{45^2 \zeta(3) M_{\text{Pl}} \lambda^2 |Y_\nu|^2 \sin^2(2\theta) m_\phi^4 (m_N^2 - 2m_\chi^2)}{1.66 \times 2^{19} \pi^6 m_N^3 (m_N^2 - m_\phi^2)^2 g_{*s} \sqrt{g_*}} \int_0^\infty T^{-1} e^{-m_N/T} dT. \quad (53)$$

The cross section for process (4),  $N\bar{N}^c \rightarrow \chi\bar{\chi}^c$ , is computed as

$$\sigma(4) = \frac{\lambda^2 \lambda'^2}{2^{12} \pi s} \sqrt{\frac{s - 4m_\chi^2}{s - 4m_N^2}} \left( \frac{\sin^2 \theta}{s - m_h^2} + \frac{\cos^2 \theta}{s - m_\phi^2} \right)^2 (s - 2m_\chi^2)(s - 2m_N^2). \quad (54)$$

Although the terms in the parenthesis adding up, this process has a non-trivial contribution only when the temperature of the singlet sector is sufficiently high, enabling efficient collisions of two right-handed neutrinos with adequate energy to produce a pair of DM particles. Given that  $m_N$  and  $m_\chi$  are significantly large, such that  $s \gg m_h^2, m_\phi^2$ , and during freeze-in  $m_N \gg T$ , we approximate  $s \sim 4m_N^2$ . Under this approximation, the thermally averaged cross section is calculated as

$$\langle \sigma v \rangle(4) = \frac{\lambda^2 \lambda'^2 \sqrt{m_\chi(m_N - m_\chi)}}{2^{13} \sqrt{2\pi} m_N^4} \left[ \left( 2m_\chi - \frac{3m_\chi^2}{2m_N} \right) + 3T \left( \frac{1}{2} + \frac{2m_\chi}{m_N} - \frac{3m_\chi^2}{2m_N^2} \right) + \frac{15T^2}{2m_N} \right], \quad (55)$$

where the relative velocity  $\sqrt{s - 4m_N^2}/m_N$  of the initial states is used. In this non-relativistic regime, the collision term is expressed as

$$C(4) = \frac{\lambda^2 \lambda'^2 \sqrt{m_\chi(m_N - m_\chi)}}{2^{14} \sqrt{2\pi} m_N^4} e^{-\frac{2m_N}{T}} T^3 \left[ \left( 2m_\chi - \frac{3m_\chi^2}{2m_N} \right) + 3T \left( \frac{1}{2} + \frac{2m_\chi}{m_N} - \frac{3m_\chi^2}{2m_N^2} \right) + \frac{15T^2}{2m_N} \right]. \quad (56)$$

Substituting this expression into the Boltzmann equation and performing the temperature integration provides the following DM yield,

$$Y_\chi(4) = \frac{45 M_{\text{Pl}} \lambda^2 \lambda'^2 (m_N^2 - 6m_\chi^2 + 8m_\chi m_N) \sqrt{m_\chi(m_N - m_\chi)}}{1.66 \times 2^{17} \sqrt{2\pi} g_{*s} \sqrt{g_*} m_N^4}. \quad (57)$$

Thus far, we have completed all necessary computations to determine the DM relic abundance. In the following sections, we present the complete expressions and proceed with a numerical analysis based on these results.

### 3.2.3 Dark matter relic density

The DM relic density, arising from both decay and scattering processes, is given by

$$\Omega_\chi h^2 = \frac{m_\chi S_0}{\rho_c / h^2} \left( \sum_{i=1}^4 Y_\chi(i) + Y_\chi \right), \quad (58)$$

where  $Y_\chi(i)$  represents the yields from the scattering processes, and  $Y_\chi$  denotes the yield from the decay processes. Utilizing this expression, we compare our theoretical predictions with the experimental measurements. For the computations, we adopt the following parameter values:  $\rho/h^2 = 1.05 \times 10^{-5} \text{ GeV cm}^{-3}$ ,  $Y_\nu = 0.1$ ,  $\theta = 10^{-5}$ ,  $m_\phi = 5 \text{ TeV}$ .

Prior to conducting a numerical analysis, we observe that the couplings  $\lambda$  and  $\lambda'$  contribute equivalently to the DM relic abundance. Specifically, exchanging these two couplings leaves the result unchanged. Based on this symmetry, we present the plots in figure 4, where we vary one coupling while keeping the other fixed, as well as varying both couplings simultaneously by the same amount. In these plots, the horizontal orange band represents the  $3\sigma$  range of the relic density as measured by Planck [57]. Any theoretical curve intersecting this band corresponds to a scenario that produces the correct amount of DM consistent with observational constraints.

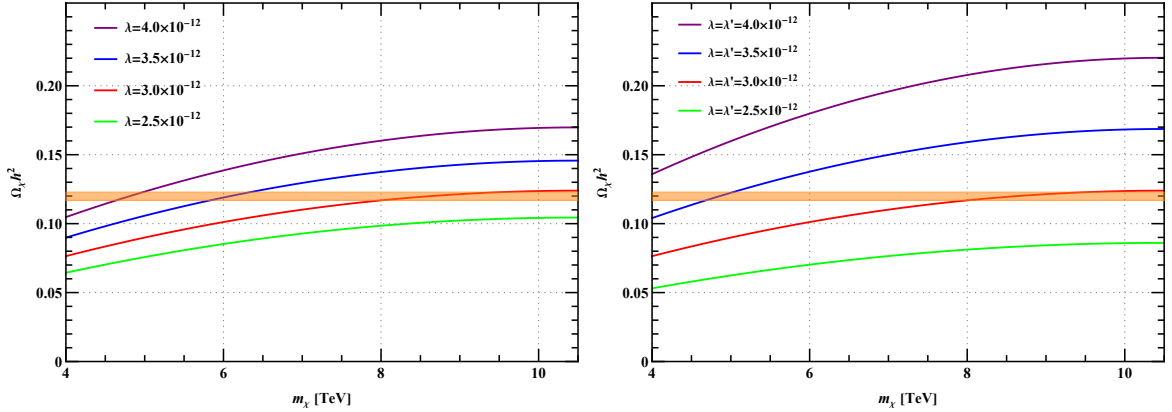


**Figure 4:** DM relic density as a function of its mass. In the left panel,  $\lambda' = 3.0 \times 10^{-12}$  is held fixed while  $\lambda$  varies among the values indicated in the legend. In the right panel, both  $\lambda$  and  $\lambda'$  are varied simultaneously by the same amount. The orange band denotes the  $3\sigma$  region of the Planck measurement [57].

In the left panel of figure 4, we fix  $\lambda' = 3.0 \times 10^{-12}$  and  $m_N = 21$  TeV, and plot the DM relic abundance as a function of its mass for different values of the coupling  $\lambda$ . As illustrated, for a given value of  $\lambda$ , the DM relic abundance reaches the experimental  $3\sigma$  range within certain intervals of the DM mass. Notably, when  $\lambda = 3.0 \times 10^{-12}$ , identical to  $\lambda'$ , the viable DM mass range is broader, spanning from 8 TeV to 10 TeV, compared to other coupling values. Conversely, for a fixed DM mass, the relic abundance increases with increasing coupling strength, indicating that the abundance of  $\chi$  freezes in more effectively with stronger interactions. If  $\lambda$  is held constant while  $\lambda'$  is varied, the resulting relic abundance remains unchanged due to the symmetric role of these couplings. In the right panel, both  $\lambda$  and  $\lambda'$  are varied simultaneously with the same value, and the qualitative behavior of the curves mirrors that of the left panel.

In figure 5, we fix  $\lambda = \lambda' = 3.0 \times 10^{-12}$  and display the DM relic density  $\Omega_\chi h^2$  as a function of the DM mass for various fixed values of the right-handed neutrino mass  $m_N$ . Each colored curve corresponds to a specific choice of  $m_N$ , with different colors representing different masses. This figure illustrates how varying the mass of the right-handed neutrino affects the relic density for a given dark matter mass. Specifically, for a fixed DM mass, the relic abundance increases as  $m_N$  increases. Larger values of  $m_N$  necessitate a larger DM mass to align the theoretical relic density with the experimental constraints. By overlaying the observational constraints (the orange band), we identify the parameter ranges that are viable for explaining the DM abundance in the Universe within the freeze-in scenario.

Through these analyses, we elucidate the interplay between the DM mass, couplings  $\lambda$

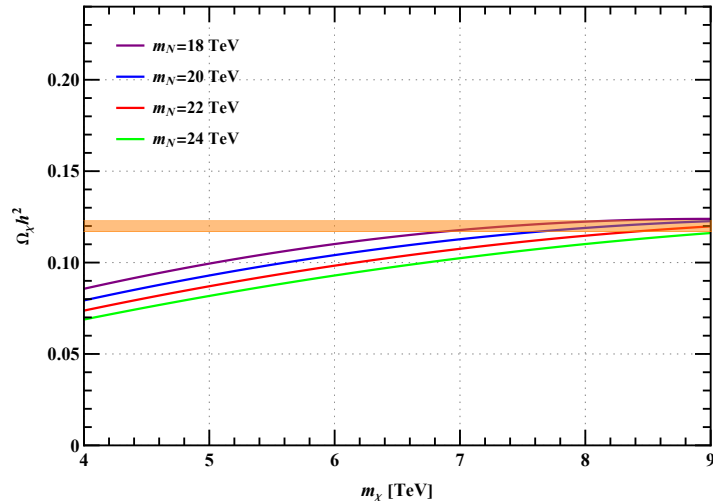


**Figure 5:** DM relic density as a function of its mass for different values of the right-handed neutrino mass  $m_N$ . We use a benchmark value  $\lambda = \lambda' = 3.0 \times 10^{-12}$  and vary  $m_N$  from 18 TeV to 24 TeV. Theoretical predictions are compared with the  $3\sigma$  Planck constraint, depicted as the orange band.

and  $\lambda'$ , and the right-handed neutrino mass  $m_N$  in determining the relic density within the freeze-in framework. The figures demonstrate that specific regions of the parameter space yield relic densities consistent with observational data, thereby identifying viable scenarios for DM production in our model.

## 4 Conclusions

In this paper, we have developed a model extending the SM by incorporating three right-handed neutrinos, three chiral fermions, and a complex scalar field, all governed by a spontaneously broken  $Z_4$  symmetry. Through this framework, we try to demonstrate that a relatively simple extension of the SM, underpinned by the discrete symmetry and the inverse seesaw mechanism, can robustly account for both the neutrino mass and the origin of DM, thereby providing a unified framework that addresses two of the most pressing puzzles in contemporary particle physics and cosmology.

Employing the inverse seesaw mechanism, our model naturally generates small neutrino masses through a double suppression involving the heavy mass scale of the right-handed neutrinos and the inherently small Majorana mass terms of the singlet fermions  $\chi_i$ . The introduction of the  $S_3$  flavor symmetry further constrains the Yukawa couplings, leading to a predictive structure for the lepton mixing matrix. Notably, the model yields specific values for the neutrino mixing angles that are close to the current experimental constraints, alongside an undetermined CP-violating phase. While these predictions exhibit qualitative agreement with current neutrino oscillation data, further refinements are necessary to achieve precise quantitative alignment.

On the DM side, the model introduces the fermion  $\chi$  as a viable DM candidate stabilized by the residual  $Z_2$  symmetry after the spontaneous breaking of  $Z_4$ . The freeze-in mechanism is realized through the feeble interactions of  $\chi$  with the other particles, predominantly facilitated by the decay and scattering processes involving the heavy singlet fermions  $N_i$ . Detailed



phenomenological analyses reveal that the model accommodates the observed relic density of DM within a plausible parameter space, characterized by appropriate choices of the couplings  $\lambda$ ,  $\lambda'$ , and the masses of the singlet fermions. Furthermore, the interplay between the heavy neutrino masses and the DM mass is mapped out, demonstrating that the model not only aligns with neutrino oscillation parameters but also naturally satisfies cosmological constraints on DM abundance.

The proposed model offers a unified solution to the simultaneous emergence of neutrino masses and DM within an extended symmetry framework. Future investigations could explore the phenomenological implications of the model in greater depth, including potential signatures at colliders and in DM detection experiments. Additionally, extending the flavor symmetry or incorporating additional symmetries might yield further insights, enhancing the model's predictive power and its concordance with emerging experimental data.

## Acknowledgements

This work is supported by the Natural Science Foundation of the Xinjiang Uyghur Autonomous Region of China under Grant No. 2022D01C52, and by the Doctoral Program of Tian Chi Foundation of the Xinjiang Uyghur Autonomous Region of China under grant No. 51052300506.

## A Perturbative diagonalization of the heavy sector mass matrix

We have implemented the first block diagonalization procedure in eqs. (23) and (22) to effectively decouple the light and heavy sectors. Subsequently, we complete the diagonalization of the heavy sector mass matrix, which is approximately represented by  $\mathcal{M}_N$  in eq. (17), to determine the masses of the newly introduced fermions. Given the hierarchical relationship  $\mu, \mu' \ll M$ , it is advantageous to employ a perturbative diagonalization technique. To facilitate this, we express the mass matrix as the sum of a dominant term and a perturbation:

$$\mathcal{M}_N \equiv \mathcal{M}_N^{(0)} + \mathcal{M}_N^{(1)} = \begin{pmatrix} 0 & M \\ M^T & 0 \end{pmatrix} + \begin{pmatrix} \mu' & 0 \\ 0 & \mu \end{pmatrix}. \quad (59)$$

Initially, we diagonalize the leading-order term. For simplicity, we assume that  $M$  is a real matrix, which can be diagonalized using two orthogonal matrices  $U_0$  and  $V_0$  through singular value decomposition,

$$M = U_0 D_0 V_0^T, \quad (60)$$

where  $D_0 = \text{diag}(\tilde{M}_1, \tilde{M}_2, \tilde{M}_3)$  is a diagonal matrix with non-negative entries,  $\tilde{M}_i \geq 0$ . Partitioning these matrices into column vectors  $\vec{u} \in U_0$  and  $\vec{v} \in V_0$ , we obtain

$$M\vec{v} = \tilde{M}\vec{u}, \quad (61)$$

$$M^T\vec{u} = \tilde{M}\vec{v}, \quad (62)$$

where  $\vec{v}$  and  $\vec{u}$  are the left and right singular vectors of  $M$ , respectively.

Next, we address the eigenvalue problem for  $\mathcal{M}_N^{(0)}$ , assuming that each eigenvector is partitioned into two  $3 \times 1$  component vectors,  $x_i$  and  $y_i$ . The eigenvalue equation is given by

$$\mathcal{M}_N^{(0)} \begin{pmatrix} \vec{x}_i \\ \vec{y}_i \end{pmatrix} = \lambda_i \begin{pmatrix} \vec{x}_i \\ \vec{y}_i \end{pmatrix}, \quad (63)$$

which expands to

$$\begin{pmatrix} 0 & M \\ M^T & 0 \end{pmatrix} \begin{pmatrix} \vec{x}_i \\ \vec{y}_i \end{pmatrix} = \lambda_i \begin{pmatrix} \vec{x}_i \\ \vec{y}_i \end{pmatrix}. \quad (64)$$

This yields the coupled equations

$$M\vec{y} = \lambda\vec{x}, \quad (65)$$

$$M^T\vec{x} = \lambda\vec{y}. \quad (66)$$

By multiplying  $M^T$  from the right side of eq. (65), we obtain

$$M^T M \vec{y} = \lambda M^T \vec{x} = \lambda^2 \vec{y}, \quad (67)$$

indicating that  $\lambda^2$  are the eigenvalues of  $M^T M$ . Similarly, from the singular value decomposition, we know that

$$M^T M \vec{v}_i = \tilde{M}_i^2 \vec{v}_i, \quad (68)$$

implying that the eigenvalues  $\lambda_i$  of  $\mathcal{M}_N^{(0)}$  are given by  $\lambda_i = \pm \tilde{M}_i$ .

Assuming all singular values  $\tilde{M}_i$  are non-zero, we first consider the case  $\lambda_i = \tilde{M}_i$ . The corresponding left eigenvector is  $\vec{y}_{(i)} = \vec{v}_{(i)}$ , and the associated  $\vec{x}_{(i)}$  is

$$\vec{x}_{(i)} = \frac{1}{\lambda_i} M \vec{y}_{(i)} = \frac{1}{\tilde{M}_i} M \vec{v}_{(i)} = \vec{u}_{(i)}. \quad (69)$$

Likewise, for  $\lambda_i = -\tilde{M}_i$ , we find

$$\vec{x}_{(i)} = \frac{1}{-\tilde{M}_i} M \vec{v}_{(i)} = -\vec{u}_{(i)}. \quad (70)$$

Thus, the eigenvectors of  $\mathcal{M}_N^{(0)}$  are

$$\left\{ \begin{pmatrix} \vec{x}_{(i)} \\ \vec{y}_{(i)} \end{pmatrix} = \begin{pmatrix} \vec{u}_{(i)} \\ \vec{v}_{(i)} \end{pmatrix}, \quad \text{for } \lambda = \tilde{M}_i; \right. \quad (71)$$

$$\left. \begin{pmatrix} \vec{x}_{(i)} \\ \vec{y}_{(i)} \end{pmatrix} = \begin{pmatrix} -\vec{u}_{(i)} \\ \vec{v}_{(i)} \end{pmatrix}, \quad \text{for } \lambda = -\tilde{M}_i. \right.$$

Although the vectors  $\vec{u}_{(i)}$  and  $\vec{v}_{(i)}$  are individually orthonormal, the combined vectors do not preserve unit normalization,

$$\left| \begin{pmatrix} \vec{x}_{(i)} \\ \vec{y}_{(i)} \end{pmatrix} \right|^2 = |\vec{x}_{(i)}|^2 + |\vec{y}_{(i)}|^2 = |\vec{u}_{(i)}|^2 + |\vec{v}_{(i)}|^2 = 2. \quad (72)$$

To rectify this, we normalize the eigenvectors

$$\begin{cases} \begin{pmatrix} \vec{x}_{(i)} \\ \vec{y}_{(i)} \end{pmatrix} = \frac{1}{\sqrt{2}} \begin{pmatrix} \vec{u}_{(i)} \\ \vec{v}_{(i)} \end{pmatrix}, & \text{for } \lambda = \tilde{M}_i; \\ \begin{pmatrix} \vec{x}_{(i)} \\ \vec{y}_{(i)} \end{pmatrix} = \frac{1}{\sqrt{2}} \begin{pmatrix} -\vec{u}_{(i)} \\ \vec{v}_{(i)} \end{pmatrix}, & \text{for } \lambda = -\tilde{M}_i. \end{cases} \quad (73)$$

The matrix  $W$  that diagonalizes  $\mathcal{M}_N^{(0)}$  thus constructed as

$$W = \frac{1}{\sqrt{2}} \begin{pmatrix} U_0 & iU_0 \\ V_0 & -iV_0 \end{pmatrix}, \quad (74)$$

where  $U_0$  and  $V_0$  are orthogonal matrices composed of the eigenvectors. It is straightforward to verify that  $W$  is a  $6 \times 6$  unitary matrix, as its columns are orthonormal eigenvectors. The diagonalization yields

$$W^T \mathcal{M}_N^{(0)} W = D_0 \oplus D_0, \quad (75)$$

indicating that, to leading order, there are three pairs of fermions, each pair possessing degenerate masses  $\tilde{M}_i$ .

To incorporate the small but non-negligible contributions from  $\mu$  and  $\mu'$ , we compute the perturbative corrections to both the eigenvalues and eigenvectors of  $\mathcal{M}_N^{(0)}$ . Our objective is to determine a unitary matrix  $Q$  and diagonal matrix  $D = \text{diag}(M_1, \dots, M_6)$  such that  $Q^T \mathcal{M}_N Q = D$ . Applying time-independent perturbation theory, the first-order correction to the eigenvalues is given by

$$\lambda_i^{(1)} = \langle \psi_i^{(0)} | \mathcal{M}_N^{(1)} | \psi_i^{(0)} \rangle, \quad (76)$$

where the unperturbed eigenvectors are

$$\begin{cases} |\psi_i^{(0)}\rangle = \frac{1}{\sqrt{2}} \begin{pmatrix} \vec{u}_{(i)} \\ \vec{v}_{(i)} \end{pmatrix}, & \text{for upper block;} \\ |\psi_i^{(0)}\rangle = \frac{1}{\sqrt{2}} \begin{pmatrix} -i\vec{u}_{(i)} \\ -i\vec{v}_{(i)} \end{pmatrix}, & \text{for lower block.} \end{cases} \quad (77)$$

The first-order correction yields identical contributions for both the positive and negative eigenvalue sectors,

$$\lambda_i^{(1)} = \frac{1}{2} \left( \vec{u}_{(i)}^\dagger \mu' \vec{u}_{(i)} + \vec{v}_{(i)}^\dagger \mu \vec{v}_{(i)} \right). \quad (78)$$

However, this uniform shift does not resolve the degeneracy between the paired fermions. Therefore, we must consider second-order corrections to lift the degeneracy

$$\lambda_i^{(2)} = \sum_{j \neq i} \frac{\left| \langle \psi_j^{(0)} | \mathcal{M}_N^{(1)} | \psi_i^{(0)} \rangle \right|^2}{\tilde{M}_i - \tilde{M}_j}, \quad (79)$$

which introduces unequal corrections to the masses within each fermion pair. Additionally, the first-order correction to the eigenvectors is given by

$$|\psi_i^{(1)}\rangle = \sum_{j \neq i} \frac{\langle \psi_j^{(0)} | \mathcal{M}_N^{(1)} | \psi_i^{(0)} \rangle}{\tilde{M}_i - \tilde{M}_j} |\psi_j^{(0)}\rangle, \quad (80)$$

which accounts for the mixing between different unperturbed eigenstates. Matrix elements in the numerators of eqs. (79) and (80) can be categorized into four distinct cases:

$$\langle \psi_j^{(0)} | \mathcal{M}_N^{(1)} | \psi_i^{(0)} \rangle = \begin{cases} \frac{1}{2} [\vec{u}_{(j)}^\dagger \mu' \vec{u}_{(i)} + \vec{v}_{(j)}^\dagger \mu \vec{v}_{(i)}], & \text{for } 1 \leq i \neq j \leq 3; \\ \frac{i}{2} [-\vec{u}_{(j)}^\dagger \mu' \vec{u}_{(i)} + \vec{v}_{(j)}^\dagger \mu \vec{v}_{(i)}], & \text{for } 1 \leq i \leq 3, 4 \leq j \leq 6; \\ \frac{i}{2} [\vec{u}_{(j)}^\dagger \mu' \vec{u}_{(i)} - \vec{v}_{(j)}^\dagger \mu \vec{v}_{(i)}], & \text{for } 4 \leq i \leq 6, 1 \leq j \leq 3; \\ \frac{1}{2} [\vec{u}_{(j)}^\dagger \mu' \vec{u}_{(i)} + \vec{v}_{(j)}^\dagger \mu \vec{v}_{(i)}], & \text{for } 4 \leq i \neq j \leq 6. \end{cases} \quad (81)$$

Ultimately, the perturbative diagonalization yields the mass matrix  $D$  for the heavy states as

$$M_i \approx \tilde{M}_i + \lambda_i^{(1)} + \lambda_i^{(2)}, \quad (82)$$

and the unitary matrix  $Q$ , whose columns are composed of the perturbed eigenvectors,

$$|\psi_i\rangle \approx |\psi_i^{(0)}\rangle + |\psi_i^{(1)}\rangle. \quad (83)$$

The unitary transformation matrix  $Q$  encapsulates the rotation from the mass basis to the flavor basis. Notably, this analysis reveals that the mixing between the fermion states  $N$  and  $S$  is significant.

## References

- [1] T. Kajita, *Nobel Lecture: Discovery of atmospheric neutrino oscillations*, *Rev. Mod. Phys.* **88** (2016) 3 030501.
- [2] A. B. McDonald, *Nobel Lecture: The Sudbury Neutrino Observatory: Observation of flavor change for solar neutrinos*, *Rev. Mod. Phys.* **88** (2016) 3 030502.
- [3] G. Bertone, D. Hooper and J. Silk, *Particle dark matter: Evidence, candidates and constraints*, *Phys. Rept.* **405** (2005) 279–390, arXiv:hep-ph/0404175.
- [4] A. Arbey and F. Mahmoudi, *Dark matter and the early Universe: a review*, *Prog. Part. Nucl. Phys.* **119** (2021) 103865, arXiv:2104.11488 [hep-ph].
- [5] M. Cirelli, A. Strumia and J. Zupan, *Dark Matter* (2024), arXiv:2406.01705 [hep-ph].
- [6] R. N. Mohapatra and J. W. F. Valle, *Neutrino Mass and Baryon Number Nonconservation in Superstring Models*, *Phys. Rev. D* **34** (1986) 1642.
- [7] A. E. Cárcamo Hernández and S. F. King, *Littlest Inverse Seesaw Model*, *Nucl. Phys. B* **953** (2020) 114950, arXiv:1903.02565 [hep-ph].
- [8] S. Centelles Chuliá, R. Srivastava and A. Vicente, *The inverse seesaw family: Dirac and Majorana*, *JHEP* **03** (2021) 248, arXiv:2011.06609 [hep-ph].
- [9] S. S. C. Law and K. L. McDonald, *Inverse seesaw and dark matter in models with exotic lepton triplets*, *Phys. Lett. B* **713** (2012) 490–494, arXiv:1204.2529 [hep-ph].
- [10] A. Abada, G. Arcadi and M. Lucente, *Dark Matter in the minimal Inverse Seesaw mechanism*, *JCAP* **10** (2014) 001, arXiv:1406.6556 [hep-ph].

- [11] A. Mukherjee and M. K. Das, *Neutrino phenomenology and scalar Dark Matter with  $A_4$  flavor symmetry in Inverse and type II seesaw*, **Nucl. Phys. B** **913** (2016) 643–663, arXiv:1512.02384 [hep-ph].
- [12] W. Abdallah, S. Choubey and S. Khan, *FIMP dark matter candidate(s) in a  $B-L$  model with inverse seesaw mechanism*, **JHEP** **06** (2019) 095, arXiv:1904.10015 [hep-ph].
- [13] C. Pongkitivanichkul, N. Thongyoi and P. Uttayarat, *Inverse seesaw mechanism and portal dark matter*, **Phys. Rev. D** **100** (2019) 3 035034, arXiv:1905.13224 [hep-ph].
- [14] S. Mandal, N. Rojas, R. Srivastava and J. W. F. Valle, *Dark matter as the origin of neutrino mass in the inverse seesaw mechanism*, **Phys. Lett. B** **821** (2021) 136609, arXiv:1907.07728 [hep-ph].
- [15] P.-H. Gu, *Inverse seesaw accompanied by Dirac fermionic dark matter*, **Phys. Lett. B** **806** (2020) 135499, arXiv:1907.11556 [hep-ph].
- [16] E. Fernandez-Martinez, M. Pierre, E. Pinsard and S. Rosauero-Alcaraz, *Inverse Seesaw, dark matter and the Hubble tension*, **Eur. Phys. J. C** **81** (2021) 10 954, arXiv:2106.05298 [hep-ph].
- [17] A. Abada et al., *Gauged inverse seesaw from dark matter*, **Eur. Phys. J. C** **81** (2021) 8 758, arXiv:2107.02803 [hep-ph].
- [18] X. Zhang and S. Zhou, *Inverse seesaw model with a modular  $S_4$  symmetry: lepton flavor mixing and warm dark matter*, **JCAP** **09** (2021) 043, arXiv:2106.03433 [hep-ph].
- [19] J. Gogoi, L. Sarma and M. K. Das, *Leptogenesis and dark matter in minimal inverse seesaw using  $A_4$  modular symmetry*, **Eur. Phys. J. C** **84** (2024) 7 689, arXiv:2311.09883 [hep-ph].
- [20] Y. b. Zeldovich, *Survey of Modern Cosmology*, **Adv. Astron. Astrophys.** **3** (1965) 241–379.
- [21] R. J. Scherrer and M. S. Turner, *On the Relic, Cosmic Abundance of Stable Weakly Interacting Massive Particles*, **Phys. Rev. D** **33** (1986) 1585, [Erratum: Phys.Rev.D 34, 3263 (1986)].
- [22] P. Gondolo and G. Gelmini, *Cosmic abundances of stable particles: Improved analysis*, **Nucl. Phys. B** **360** (1991) 145–179.
- [23] G. Steigman, B. Dasgupta and J. F. Beacom, *Precise Relic WIMP Abundance and its Impact on Searches for Dark Matter Annihilation*, **Phys. Rev. D** **86** (2012) 023506, arXiv:1204.3622 [hep-ph].
- [24] M. Schumann, *Direct Detection of WIMP Dark Matter: Concepts and Status*, **J. Phys. G** **46** (2019) 10 103003, arXiv:1903.03026 [astro-ph.CO].
- [25] R. Frumkin, E. Kuflik, I. Lavie and T. Silverwater, *Roadmap to Thermal Dark Matter beyond the Weakly Interacting Dark Matter Unitarity Bound*, **Phys. Rev. Lett.** **130** (2023) 17 171001, arXiv:2207.01635 [hep-ph].
- [26] P. de la Torre, M. Gutiérrez and M. Masip, *Monochromatic neutrinos from dark matter through the Higgs portal*, **JCAP** **11** (2023) 068, arXiv:2309.00374 [hep-ph].

- [27] L. J. Hall, K. Jedamzik, J. March-Russell and S. M. West, *Freeze-In Production of FIMP Dark Matter*, **JHEP** **03** (2010) 080, arXiv:0911.1120 [hep-ph].
- [28] F. Elahi, C. Kolda and J. Unwin, *UltraViolet Freeze-in*, **JHEP** **03** (2015) 048, arXiv:1410.6157 [hep-ph].
- [29] A. Biswas and A. Gupta, *Freeze-in Production of Sterile Neutrino Dark Matter in  $U(1)_{B-L}$  Model*, **JCAP** **09** (2016) 044, [Addendum: JCAP 05, A01 (2017)], arXiv:1607.01469 [hep-ph].
- [30] N. Bernal et al., *The Dawn of FIMP Dark Matter: A Review of Models and Constraints*, **Int. J. Mod. Phys. A** **32** (2017) 27 1730023, arXiv:1706.07442 [hep-ph].
- [31] M. Chianese and S. F. King, *The Dark Side of the Littlest Seesaw: freeze-in, the two right-handed neutrino portal and leptogenesis-friendly fimpzillas*, **JCAP** **09** (2018) 027, arXiv:1806.10606 [hep-ph].
- [32] M. Becker, *Dark Matter from Freeze-In via the Neutrino Portal*, **Eur. Phys. J. C** **79** (2019) 7 611, arXiv:1806.08579 [hep-ph].
- [33] M. Chianese, B. Fu and S. F. King, *Minimal Seesaw extension for Neutrino Mass and Mixing, Leptogenesis and Dark Matter: FIMPzillas through the Right-Handed Neutrino Portal*, **JCAP** **03** (2020) 030, arXiv:1910.12916 [hep-ph].
- [34] R. Allahverdi and J. K. Osiński, *Freeze-in Production of Dark Matter Prior to Early Matter Domination*, **Phys. Rev. D** **101** (2020) 6 063503, arXiv:1909.01457 [hep-ph].
- [35] C. Cosme et al., *Neutrino portal to FIMP dark matter with an early matter era*, **JHEP** **03** (2021) 026, arXiv:2003.01723 [hep-ph].
- [36] C. E. Yaguna and O. Zapata, *Minimal model of fermion FIMP dark matter*, **Phys. Rev. D** **109** (2024) 1 015002, arXiv:2308.05249 [hep-ph].
- [37] A. Abada et al., *Thermal effects in freeze-in neutrino dark matter production*, **JHEP** **11** (2023) 180, arXiv:2308.01341 [hep-ph].
- [38] X.-J. Xu, S. Zhou and J. Zhu, *The  $\nu_R$ -philic scalar dark matter*, **JCAP** **04** (2024) 012, arXiv:2310.16346 [hep-ph].
- [39] M. Schmaltz and N. Weiner, *A Portalino to the Dark Sector*, **JHEP** **02** (2019) 105, arXiv:1709.09164 [hep-ph].
- [40] C. E. Yaguna and O. Zapata, *Multi-component scalar dark matter from a  $Z_N$  symmetry: a systematic analysis*, **JHEP** **03** (2020) 109, arXiv:1911.05515 [hep-ph].
- [41] C. E. Yaguna and O. Zapata, *Two-component scalar dark matter in  $Z_{2n}$  scenarios*, **JHEP** **10** (2021) 185, arXiv:2106.11889 [hep-ph].
- [42] D. Hepburn and S. M. West, *Dark matter and neutrino masses in a Portalino-like model*, **Eur. Phys. J. C** **83** (2023) 5 405, arXiv:2208.02698 [hep-ph].
- [43] A. Liu, Z.-L. Han, Y. Jin and H. Li, *Sterile neutrino portal dark matter with  $Z_3$  symmetry*, **Phys. Rev. D** **108** (2023) 7 075021, arXiv:2306.14091 [hep-ph].

- [44] G. 't Hooft, *Naturalness, chiral symmetry, and spontaneous chiral symmetry breaking*, *NATO Sci. Ser. B* **59** (1980) 135–157.
- [45] S. Weinberg, *Baryon and Lepton Nonconserving Processes*, *Phys. Rev. Lett.* **43** (1979) 1566–1570.
- [46] T. Robens and T. Stefaniak, *Status of the Higgs Singlet Extension of the Standard Model after LHC Run 1*, *Eur. Phys. J. C* **75** (2015) 104, arXiv:1501.02234 [hep-ph].
- [47] G. Dupuis, *Collider Constraints and Prospects of a Scalar Singlet Extension to Higgs Portal Dark Matter*, *JHEP* **07** (2016) 008, arXiv:1604.04552 [hep-ph].
- [48] P. Bechtle et al., *HiggsSignals-2: Probing new physics with precision Higgs measurements in the LHC 13 TeV era*, *Eur. Phys. J. C* **81** (2021) 2 145, arXiv:2012.09197 [hep-ph].
- [49] S. D. Lane, I. M. Lewis and M. Sullivan, *Resonant multiscalar production in the generic complex singlet model in the multi-TeV region*, *Phys. Rev. D* **110** (2024) 5 055017, arXiv:2403.18003 [hep-ph].
- [50] H. Ishimori et al., *Non-Abelian Discrete Symmetries in Particle Physics*, *Prog. Theor. Phys. Suppl.* **183** (2010) 1–163, arXiv:1003.3552 [hep-th].
- [51] P. P. Novichkov, J. T. Penedo, S. T. Petcov and A. V. Titov, *Generalised CP Symmetry in Modular-Invariant Models of Flavour*, *JHEP* **07** (2019) 165, arXiv:1905.11970 [hep-ph].
- [52] I. Esteban et al., *NuFit-6.0: Updated global analysis of three-flavor neutrino oscillations* (2024), arXiv:2410.05380 [hep-ph].
- [53] *NuFit webpage*, <http://www.nu-fit.org>.
- [54] S. Navas et al. (Particle Data Group), *Review of particle physics*, *Phys. Rev. D* **110** (2024) 3 030001.
- [55] J. McDonald, *Thermally generated gauge singlet scalars as selfinteracting dark matter*, *Phys. Rev. Lett.* **88** (2002) 091304, arXiv:hep-ph/0106249.
- [56] G. Bélanger et al., *micrOMEGAs5.0 : Freeze-in*, *Comput. Phys. Commun.* **231** (2018) 173–186, arXiv:1801.03509 [hep-ph].
- [57] N. Aghanim et al. (Planck), *Planck 2018 results. VI. Cosmological parameters*, *Astron. Astrophys.* **641** (2020) A6, [Erratum: *Astron. Astrophys.* 652, C4 (2021)], arXiv:1807.06209 [astro-ph.CO].